Research Article Open Access

Edwin Ostertag*, Anita Lorenz, Karsten Rebner, Rudolf W. Kessler, Alfred J. Meixner

Extension of solid immersion lens technology to super-resolution Raman microscopy

Abstract: Scanning Near-Field Optical Microscopy (SNOM) has developed during recent decades into a valuable tool to optically image the surface topology of materials with super-resolution. With aperture-based SNOM systems, the resolution scales with the size of the aperture, but also limits the sensitivity of the detection and thus the application for spectroscopic techniques like Raman SNOM. In this paper we report the extension of solid immersion lens (SIL) technology to Raman SNOM. The hemispherical SIL with a tip on the bottom acts as an apertureless dielectric nanoprobe for simultaneously acquiring topographic and spectroscopic information. The SIL is placed between the sample and the microscope objective of a confocal Raman microscope. The lateral resolution in the Raman mode is validated with a cross section of a semiconductor layer system and, at approximately 180 nm, is beyond the classical diffraction limit of Abbe.

Keywords: solid immersion lens, near-field, SNOM, nanoscopy, super-resolution, Raman spectroscopy, diffraction limit, chemical imaging, BAM L-200 reference pattern

DOI 10.2478/nansp-2014-0001
Received June 22, 2014; accepted October 8, 2014

***Corresponding author: Edwin Ostertag:** Process Analysis & Technology, Reutlingen Research Institute, Reutlingen University, Alteburgstr. 150, D-72762 Reutlingen, E-mail: edwin.ostertag@reutlingen-university.de
Anita Lorenz, Karsten Rebner, Rudolf W. Kessler: Process Analysis & Technology, Reutlingen Research Institute, Reutlingen University, Alteburgstr. 150, D-72762 Reutlingen
Alfred J. Meixner: Institute for Physical and Theoretical Chemistry, Auf der Morgenstelle 18, University of Tübingen, D-72076 Tübingen

1 The near-field accessed with solid immersion lens technology

The main reason for using solid immersion lenses is their capability to enhance the spatial resolution. Solids have higher refractive indices than air. When used as the immersion medium, light travels more slowly and the wavelength is shorter in the optically denser medium which results in an improvement in resolution. Mansfield and Kino were the first to recommend the SIL for increasing the spatial resolution of the optical microscope [1]. A SIL is a spherical lens (diameter 2r, refractive index n_{SIL}) which is polished to a thickness of r (hemisphere type) or $(1+1/n_{SIL})r$ (supersphere or Weierstrass type) [2,3]. The sphere diameter is usually in the range of single millimeters down to micrometers. The numerical aperture (NA) of the complete system is improved by factor of n_{SIL} (hemisphere type) or $(n_{SIL})^2$ (Weierstrass type) – subject to the condition that the refractive index of the substrate is at least as high as the refractive index of the SIL. If this condition is not met, the refractive index of the substrate limits the effective numerical aperture NA_{eff} of the SIL/objective optical system (with $NA_{eff} = n_{SIL} \sin\alpha_m$, where α_m is the marginal ray angle inside the SIL) [4]. The angular range of collected information is determined by the SIL probe, the objective lens, and the detector [5].

The SIL technique is also known as "numerical aperture increasing lens (NAIL) microscopy" [6]. For the NAIL technique the inclusion of evanescent waves is crucial for resolution gain [7]. Tom Milster *et al.* have described the role of propagating and evanescent waves in solid immersion lens systems [8].

It must be emphasized here that the lateral resolution of a SIL microscope can exceed the "NAIL Limit", i.e. by the factor of the refractive index n_{SIL}. In order to achieve this, the evanescent component of the light from the substrate has to be identified amongst the predominant propagated component. One approach is to tailor the angular spectrum by annular illumination and collection which can significantly improve the resolution and emphasize

© 2014 Edwin Ostertag et al., licensee De Gruyter Open.
This work is licensed under the Creative Commons Attribution-NonCommercial-NoDerivs 3.0 License.
Bereitgestellt von | Hochschule Reutlingen
Angemeldet
Heruntergeladen am | 01.10.15 12:18

the upper layer of a substrate [9]. This corresponds in principle to a dark field illumination scheme. Another approach uses aperture diaphragms for illumination and detection which are independent of each other. Based on the latter approach, a high lateral resolution of the SIL SNOM technique of 30 nm using primary light (not frequency shifted like Raman radiation) on semiconductor test structures has been demonstrated [10].

A particular advantage of the SIL technique is the high collection efficiency. Koyama estimates the collection efficiency with an NA = 0.8 objective and an n = 1.845 SIL to be about 60%-70%, which well exceeds the diffraction-limited value of 50% for 2π-solid angle collection in conventional methods [11]. This high collection efficiency makes the SIL technique highly suitable for applications of Raman spectroscopy or other spectroscopic techniques.

Solid immersion lenses vary greatly with diameters from millimeters to micrometers. SILs with diameters in the micrometer region [12] down to sub-wavelength size [13] are described in the literature. Brunner *et al.* propose a diffraction-based solid immersion lens (dSIL) as an alternative to the conventional design based on refraction [14]. Frey *et al.* show back-illuminated full body glass tips coated with a thin metal layer. They can be used as apertureless optical nanoprobes for scanning near-field optical microscopy with high spatial resolution down to 15 nm at high electrical field intensities [15]. A tip-enhanced SIL (TESIL) combines a SIL with a nano metal particle for local field enhancement [16].

The development of applications for the SIL technique is driven by optical data storage [17-21] and wafer inspection systems in semiconductor processing [22,23]. Further applications include high-resolution imaging [24-27], lithography [28,29] and spectroscopy [24,30].

The extension of SIL technology for super-resolution Raman microscopy is not common, especially in combination with scanning probe microscopy. Near-field spectroscopy combined with Raman scattering offers chemical information at high spatial resolution. Nevertheless the performance is limited due to some inherent as well as technical problems like a long scanning time and rather weak Raman signals [31].

A SIL as optical nanoprobe for super-resolution Raman microscopy and spectroscopy has the potential to maintain the high intensity throughput of a lens in combination with a lateral resolution below the diffraction limit [32]. Less than 5 references for this Raman SIL approach could be found in literature by the authors. Athalin *et al.* [33] use a supersphere SIL to perform Raman spectroscopy with enhanced resolution of nanovolume samples like Ag colloids. Desmedt *et al.* integrate a nanolens into a confocal Raman microscope to enhance the Raman scattering signal [34]. Poweleit *et al.* perform Raman imaging of patterned silicon with a 3 mm diameter SIL and report a sub-500 nm lateral resolution [35]. Lerman *et al.* apply SIL near-field optics to the Raman analysis of strained silicon films. Their approach consists of forming a SIL with diameters from 15 - 40 µm at the edge of an optical fiber which can be combined with an AFM system [32]. The achievable spatial resolution with this system is not given.

In this paper we present the integration of a solid immersion lens in a flexible metal cantilever with a commercially available confocal Raman microscope.

2 Optical setup of the Raman SNOM imaging and spectroscopy system

2.1 Selection of the SIL concept

Fig. 1 shows various SIL shapes: a) is a hemispherical SIL with a flat base; b) represents a supersphere (Weierstrass) type, also with a flat base. Types c) and d) differ from the previous ones in that the base has a conical tip with various point angles. The SIL presented in this paper has a point angle of 130°. The advantage of the c) and d) designs is that in addition to the chemistry-related optical information, morphology-related topographic information may also be gathered. Type e) presents a hemispherical SIL with a conical dielectric probe which can achieve higher performance in terms of high throughput and lower reflection of the light beam than the conventional metal SNOM probe or SIL used alone [5]. Thus the shape of this SIL is related to the types c) and e) with conical tips. The shape of diffractive solid immersion systems (Fig. 1 b) deviates from the spherical design of previous SILs [14,36].

The concept of a solid immersion lens as a scanning probe for SNOM was developed some years ago by Ghislain *et al.* [37]. In this development, monochromatic laser light or polychromatic light is injected through an objective (50 x 0.55 NA) in a SIL and recorded by a photodetector. Because of the high transmission through the lens, the SIL system ensures an improvement of the signal-to-noise (S/N) ratio in comparison to aperture-limited systems. A SIL probe producing a spot size of about 100 nm transmits about half (50%) of the optical power [25,28,38]. By comparison, a metal-coated fiber-probe with a 100 nm aperture transmits only a tiny fraction (10^{-3} - 10^{-6}) of the light coupled into the fiber [16, 39-41]. The high S/N ratio is a prerequisite for performing near-field optical

Bereitgestellt von | Hochschule Reutlingen
Angemeldet
Heruntergeladen am | 01.10.15 12:18

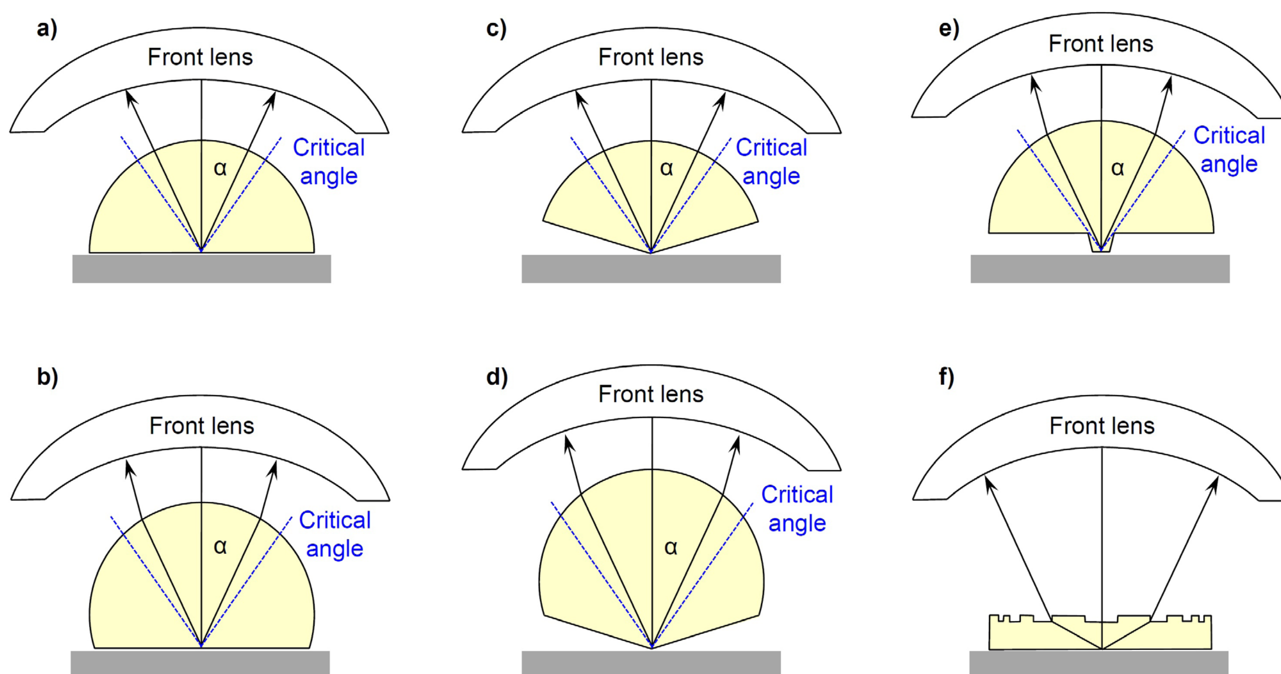

Figure 1: Solid immersion lens (SIL) types. All SILs are located on a substrate and positioned below the front lens of a microscope objective. a) hemisphere with flat bottom, b) supersphere (Weierstrass) with flat bottom, c) hemisphere with conical tip, d) supersphere with conical tip, e) hemispherical SIL with a conical dielectric probe. a) e) the critical angles of total internal refection are illustrated. f) diffraction-based SIL (by courtesy of Robert Brunner, modified [14]).

spectroscopy. Recent work showed that the SIL-system enhances the lateral resolution under primary light irradiation up to 30 nm and improves the S/N ratio due to the high transmission efficiency [10,24,42]. Because of these advantages the hemispherical SIL with a conically sanded tip on the bottom (Fig. 1 c) was chosen as the starting point for integration into a Raman microscope.

2.2 Integration into a standard Raman microscope

The goal is a convenient integration of the SIL near-field unit into a standard Raman microscope for simple operation. The setup consists of an alpha300 SR Raman microscope from WITec GmbH. The top microscope is a Zeiss Axio Scope A1. A piezo table is used as a microscope stage, under which the illumination unit is situated. A total of 3 CCD cameras enable a view of the sample from above (ocular camera), the side and underneath. The sample is illuminated by a LED white light source.

For diffraction-based Raman imaging and spectroscopy, a spectrograph with two selectable gratings is available which is lens-based and optimized for maximum illumination intensity (WITec UHTS 300). The Raman signal is recorded by a highly sensitive, back-illuminated CCD matrix detector, Peltier cooled to -60°C, with optional EM mode (VIS optimized Andor Newton EMCCD). The source for Raman excitation is a frequency-doubled Nd:YAG laser ($\lambda = 532$ nm). In addition, the system contains a complete AFM unit with which the sample is scanned underneath the fixed nanoprobe. The tip holder of the probe has its own piezo drive in x-, y- and z-direction for correct positioning.

For Raman imaging and spectroscopy beyond the diffraction limit, the system does not use the commercially available aperture limited pinhole tips for SNOM. Instead, a solid immersion lens with a conically shaped tip on the bottom is used as a nanoprobe. Fig. 2 a depicts the integration of the SIL in a flexible metal foil cantilever underneath the microscope objective.

2.3 SIL tip for Raman spectroscopy and imaging

The design of the SIL responds to the needs of an optical probe for SPM. The SIL consists of a hemispheric lens with a diameter of 0.1 cm and a conically sanded tip at the bottom with a point angle of 130°. The tip forms the scanning probe with a tip radius of roughly 700 nm (Fig. 2 b). The front view reveals helical scrub marks from classical lens grinding technology on the outside of the apex (c). Depending on the wavelength range of

Bereitgestellt von | Hochschule Reutlingen
Angemeldet
Heruntergeladen am | 01.10.15 12:18

interest, SILs of different materials are used: sapphire, cubic zirconium oxide and gallium phosphide for the NIR. The SIL is mounted on a cantilever. The cantilever consists of a flexible metal foil with a side mirror at the end. This specific SIL cantilever design has originally been published and patented by Ghislain *et al.* at Veeco Instruments [37,44].

Fig. 2 d shows how the SIL cantilever is magnetically attached to a holder with a piezo drive to enable tip movements in x-, y- and z-axis. The sample itself can be scanned by the piezo stage. The SIL-cantilever is in contact with the sample surface. A specific beam deflection setup was developed to record the deflection of the cantilever: a laser beam is directed from the side onto the cantilever mirror. The reflected light is detected by a segmented photodiode with 4 quadrants. SNOM measurements both in reflection and transmission modes are possible.

Due to the multimodal setup of the whole system, the optical signal collected by the SIL can be either recorded by a PMT (records only the intensity) or can be spectrally resolved by a Raman spectrometer. Thus, Raman imaging is possible with enhanced lateral resolution.

3 Validation of the lateral resolution with reference pattern

3.1 Reference pattern BAM L-200

The reference pattern BAM L-200 is used to determine the lateral resolution of the solid immersion lens setup. The test pattern has been available from the Bundesanstalt für Materialforschung (BAM) since 2007 for structure sizes below 100 nm [45]. The stripe pattern is manufactured by metalorganic vapour phase epitaxy (MOVPE) of GaAs-$Al_{(0.7)}Ga_{(0.3)}As$-$In_{(0.2)}Ga_{(0.8)}As$ layers on a GaAs substrate. The cross-section polish of the semiconductor layers offers a material contrast on a plane surface with extreme low topography. It comprises 142 layers, inter alia grids with 3 stripes with periods from 2 nm to 600 nm.

The BAM L-200 reference pattern with its semiconductor layers GaAs and $Al_{(0.7)}Ga_{(0.3)}As$ exhibits an optical contrast under visible light illumination, and so the test pattern is suitable for determining the spatial resolution of a SIL system in the VIS range [10,24].

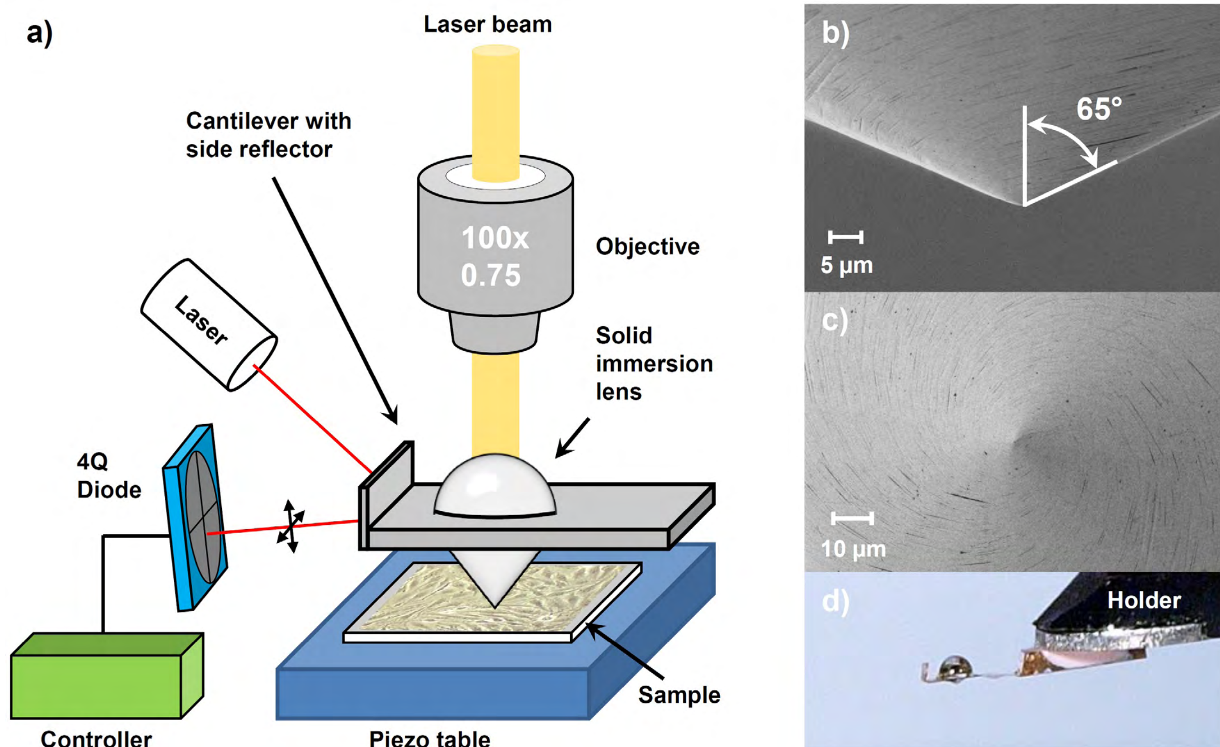

Figure 2: a) Apertureless near-field option with solid immersion lens cantilever for operation in backscattering and transmission mode. The near-field unit is installed below the microscope objective. The sample can be scanned by the piezo stage. A specific beam deflection setup with a laser beam from the left side monitors the deflection of the cantilever. The diagram is not to scale. b) Side view of the tip apex with an angle of 130° on the bottom of the SIL. c) Front view of the apex. Helical scrub marks from classical grinding technology remain from the production process. SEM images b) and c) by courtesy of Birgit Schröppel, NMI [43]. d) SIL tip mounted on metal foil cantilever. The cantilever is magnetically attached to the holder which itself can be moved by a piezo in x-, y- and z-axis directions.

Bereitgestellt von | Hochschule Reutlingen
Angemeldet
Heruntergeladen am | 01.10.15 12:18

3.2 Raman spectra

The optical phonon modes of GaAs and $Al_{(0.7)}Ga_{(0.3)}As$ lattices can be measured with Raman spectroscopy and provide in this way a chemical contrast. Fig. 3 presents Raman spectra from confocal measurements. Depending on the crystal planes (100), (111), (110) specific phonon modes are observed [46,47]. The BAM L-200 sample features a Raman band at 269 cm^{-1} for the GaAs segments. It is assigned to a transverse optical mode (TO) and belongs to the GaAs-like modes [48-50]. In the Raman spectrum of $Al_{(0.7)}Ga_{(0.3)}As$ two further bands are detected: the band at 366 cm^{-1} shift is assigned to a TO mode and the band at 393 cm^{-1} to a longitudinal optical mode (LO). The modes belong to the AlAs-like modes [51-53].

The refractive indices of GaAs (3.3) and $Al_{(0.7)}Ga_{(0.3)}As$ (3.7) are large enough to not limit the effective aperture of the system objective plus SIL by an inappropriate selection of the substrate [6,8]. Thus the BAM L-200 pattern is chosen for determining the spatial resolution of the SIL system in the Raman mode.

3.3 Lateral resolution

Fig. 4 a shows the scheme of the pattern of our area of interest with the corresponding scale information in Fig. 2 b. The optical signal from the SIL is recorded with a PMT during scanning across the surface with polychromatic illumination. The resulting image is illustrated in Fig. 4 c. After the localization of the area of interest, a Raman line scan is performed along the marked black line. Complete Raman spectra are acquired for every local point of the line scan. The cross section represented in Fig. 4 d is recorded with SIL and is extracted only from the intensity of the Raman band at $\tilde{\nu}$ = 365 cm^{-1}. The band at 365 cm^{-1} is characteristic for the $Al_{(0.7)}Ga_{(0.3)}As$ segments and differentiates them from the GaAs layers. The Raman spectra are corrected for background luminescence applying a fifth order polynomial to determine the intensities at 365 cm^{-1} shift. The cross section is then calculated based on the Raman shift mentioned above. In the following step the cross-section is smoothed (2nd order, 4 points). In Fig. 4 the cross section is aligned under the corresponding stripes for easy comparison (d). At first, the

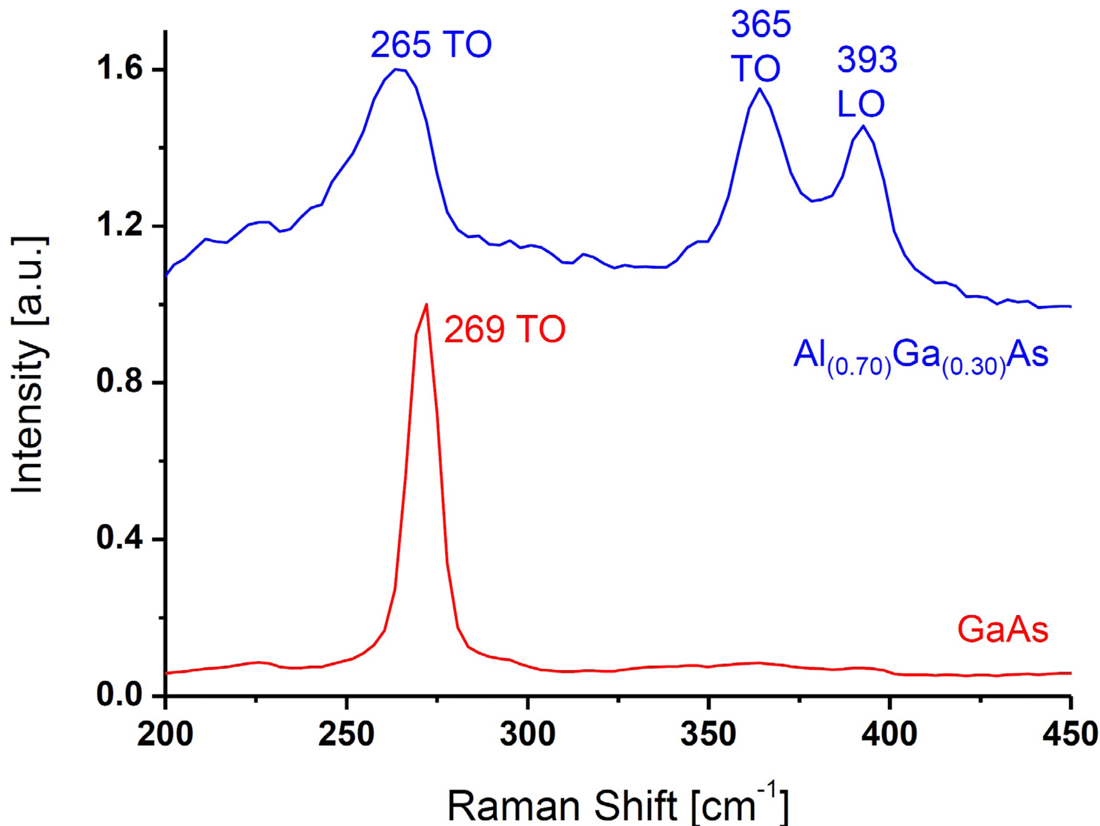

Figure 3: Raman spectra of GaAs and $Al_{(0.70)}Ga_{(0.30)}As$ segments of the BAM L200 reference pattern. The bands at 256 cm^{-1} and 269 cm^{-1} are assigned to transverse optical (TO) phonon modes of the GaAs-like modes. The band at 365 cm^{-1} is assigned to a TO phonon mode, the band at 393 cm^{-1} to a longitudinal optical (LO) mode. Both belong to the AlAs-like modes. Spectra are vertically displaced.

Bereitgestellt von | Hochschule Reutlingen
Angemeldet
Heruntergeladen am | 01.10.15 12:18

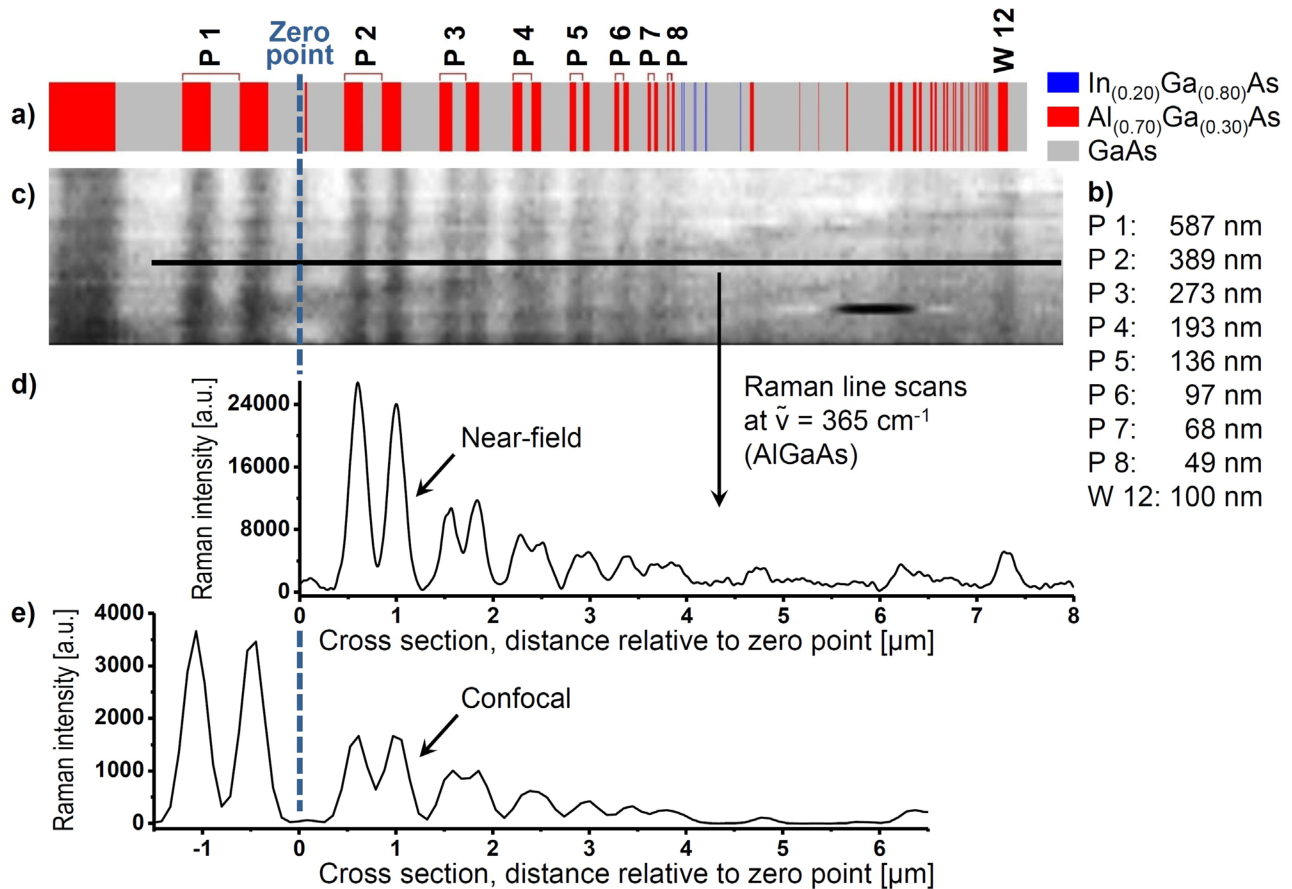

Figure 4: Raman imaging with solid immersion lens. a) Diagram of BAM L-200 reference pattern (by courtesy of Bundesanstalt für Materialforschung [45]). The periods of the stripe patterns P 1 to P 8 are labeled. A color code indicates the material of the stripes. b) Period lengths of P 1 to P 8 and width of stripe W 12. c) Optical PMT signal via SIL of an area scan of the reference pattern. d) Raman line scan with SIL covering the structures from P 2 to W 12 over a distance of 8 µm. e) Confocal Raman line scan without SIL covering the structures from P 1 to P 8 over a distance of 8 µm. Both cross sections d) and e) are evaluated on the intensity of the Raman band at $\tilde{\nu}$ = 365 cm^{-1} shift after luminescence background correction and smoothing.

smallest resolvable line pair with SIL is P 5 (half period 68 nm). The cross-section of a confocal Raman line scan is presented in section e). The smallest resolvable line pair is P 3 (half period 137 nm). The BAM L-200 pattern cannot be measured in the confocal mode with full laser power to avoid damage. It is noteworthy that the SIL helps to conserve samples due to an indirect interaction of the incident light with the sample.

The lateral resolution of the SIL in the Raman mode can be determined more quantitatively with the modulation transfer function (MTF). The optical transfer function (OTF) is the Fourier transform of the imaging system´s point spread function. A concise insight is given in the standard DIN ISO 9334 - Definitions and mathematical relationships [54]. For determining the lateral resolution in surface analytical methods, only the MTF is of relevance.

3.4 Contrast

Contrast in an optical image refers to the difference between bright and dark regions. More generally, the difference between maximum and minimum of sinusoidal periodic variables is denoted modulation. Fig. 5 describes the definition of the image contrast or modulation as

$$m_i = \frac{I_{\max} - I_{\min}}{I_{\max} + I_{\min}} \tag{1}$$

for a sinusoidal object pattern.

Comparing the modulation m_i of an image to the modulation m_o of the object by merely dividing m_i by m_o results in a single number:

$$MTF = m_i / m_o \tag{2}$$

Bereitgestellt von | Hochschule Reutlingen
Angemeldet
Heruntergeladen am | 01.10.15 12:18

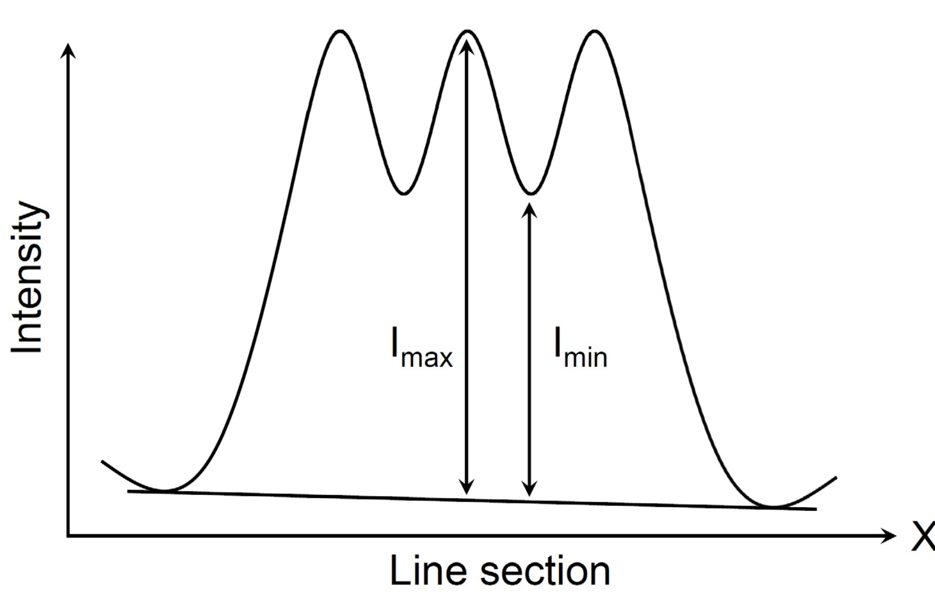

Figure 5: Definition of the image contrast or modulation as $m_i = (I_{max} - I_{min}) / (I_{max} + I_{min})$.

The number between 0 and 1 characterizes the imaging properties in terms of contrast transfer or modulation transfer.

Table 1 presents the investigated stripes on the BAM L-200 reference system. The maximum (I_{max}) and minimum (I_{min}) Raman intensities at $\tilde{\nu}$ = 365 cm^{-1} are listed as I_{max} and I_{min} (see Fig. 5). The image contrast or modulation m_i / m_o is given in the last column, calculated according to equation (1). The modulation of the object m_o is calculated from a position on the sample, where the lateral resolution is still not limited (P 2).

Table 2 presents the stripes of the reference pattern measured by confocal Raman spectroscopy with a 100x objective and a confocal pinhole of 25 µm diameter (corresponding to the collection fiber diameter). The imaged maximum (I_{max}) and minimum (I_{min}) Raman intensities at $\tilde{\nu}$ = 365 cm^{-1} shift are listed again as I_{max} and I_{min}. The modulation m_i / m_o is given in the last column.

Fig. 6 shows the corresponding modulation transfer functions for a measurement with the SIL (left) and for the confocal case without SIL (right).

For the case with the SIL the lateral resolution $\Delta x_{||}$ according to Rayleigh (m_i / m_o = 0.15) [55] is determined to 175 nm (5.7 μm^{-1}). A calculation with n_{SIL} = 2.18 for ZrO_2, $NA_{Objective}$ = 0.75 and λ = 532 nm yields for

Table 1: Stripes of the BAM L-200 reference pattern investigated by SIL and Raman spectroscopy at $\tilde{\nu}$ = 365 cm^{-1}. Intensities I_{max} and I_{min} of the cross section from Fig. 4 d are given. The last column lists the modulation m_i / m_o.

Element #	Period [nm]	Stripe [nm]	Period [µm⁻¹]	Imax [cts]	Imin [cts]	mi / mo
P 2	389	195	2.6	25711	2649	1.00
P 3	273	137	3.7	10769	4419	0.52
P 4	193	97	5.2	6348	4569	0.20
P 5	136	68	7.4	4233	3608	0.10
P 6	97	49	10.3	not resolved		0

Table 2: Stripes of the BAM L-200 reference pattern investigated by confocal Raman spectroscopy at $\tilde{\nu}$ = 365 cm^{-1} shift (100x objective, 25 µm detection fiber). Intensities I_{max} and I_{min} of the cross section from Fig. 4 d) are given. The last column lists the modulation m_i / m_o.

Element #	Period [nm]	Stripe [nm]	Period [µm⁻¹]	Imax [cts]	Imin [cts]	mi / mo
P 1	587	294	1.7	3561	323	1.00
P 2	389	195	2.6	1666	644	0.53
P 3	273	137	3.7	1005	850	0.10
P 4	193	97	5.2	not resolved		0

Bereitgestellt von | Hochschule Reutlingen
Angemeldet
Heruntergeladen am | 01.10.15 12:18

$$\Delta x_{||} = 0.61\frac{\lambda}{NA} = 0.61\frac{\lambda}{NA_{objective}n_{SIL}} = 198 \text{ nm} \quad (3)$$

which is in good agreement with the measured value. The value, slightly better measured than the calculated value, implies that the reference is perfectly suitable. Additionally, the effective numerical aperture

$$NA_{eff} = NA_{objective}n_{SIL} \quad (4)$$

might also be marginally higher than assumed. The lateral resolution according to Sparrow (m_i / m_o ≥ 0) [55] is determined to 93 nm (10.2 µm^{-1}).

For the confocal case without SIL (Fig. 6 right) the lateral resolution $\Delta x_{||}$ according to Rayleigh is determined to 286 nm (3.5 µm^{-1}). The calculation results in

$$\Delta x_{||} = 0.61\frac{\lambda}{NA\sqrt{2}} = 306 \text{ nm} \quad (5)$$

with λ = 532 nm and NA = 0.75. The factor $\sqrt{2}$ describes in a simplified way the improvement of the lateral resolution in confocal microscopy compared to wide-field microscopy [56]. The improvement for Rayleigh two-point resolution by a factor of $\sqrt{2}$ is an optimistic approximation [57,58]. The calculated result is in good agreement with the measurement. The lateral resolution according to Sparrow is determined to 192 nm (5.2 µm^{-1}).

The experimental result for the lateral resolution in the SIL Raman mode with approximately 180 nm is slightly better than expected for the immersion effect with approximately 200 nm. Solid immersion is also referred to as numerical aperture increasing lens / NAIL effect [22]. Even for the NAIL effect, the inclusion of evanescent waves is crucial for the resolution gain [8]. In the present experiment the lateral resolution in the Raman mode with SIL is not as high as under primary irradiation (no frequency shift). Firstly, the separation of the evanescent waves from the propagating waves is sub-optimal, secondly, the distance between the SIL and the sample is not less than the evanescent field decay length [17] which is a prerequisite for high resolution imaging and thirdly, the evanescent waves collected with the SIL are trapped in the space of the SIL and can only partly exit it.

In their paper "Applying solid immersion near-field optics to Raman analysis of strained silicon thin films", Lerman *et al.* [32] demonstrate a lateral resolution of their µ-SIL of 140 nm in the primary light mode (with a laser wavelength of 532 nm and n_{SIL} = 1.9). For the Raman operation mode a lateral resolution is not given.

Poweleit at al. [35] present a lateral resolution in the SIL Raman imaging mode of sub 500 nm (with a laser wavelength of 532 nm an n_{SIL} = 1.868).

Compared to the above value, the lateral resolution of approximately 180 nm of the SIL in Raman imaging mode in our setup is better. It is, moreover, clearly beyond the classical diffraction limit of Abbe.

4 Conclusions

The extension of solid immersion lens technology to Raman SNOM by integrating a Ghislain-type SIL to a confocal Raman microscope is demonstrated.

In previous work a solid immersion lens is used in an early Zeiss UMSP 80 microspectrophotometer under primary light irradiation (not frequency shifted) for imaging and spectroscopy with a lateral resolution in the range of 30 nm [24].

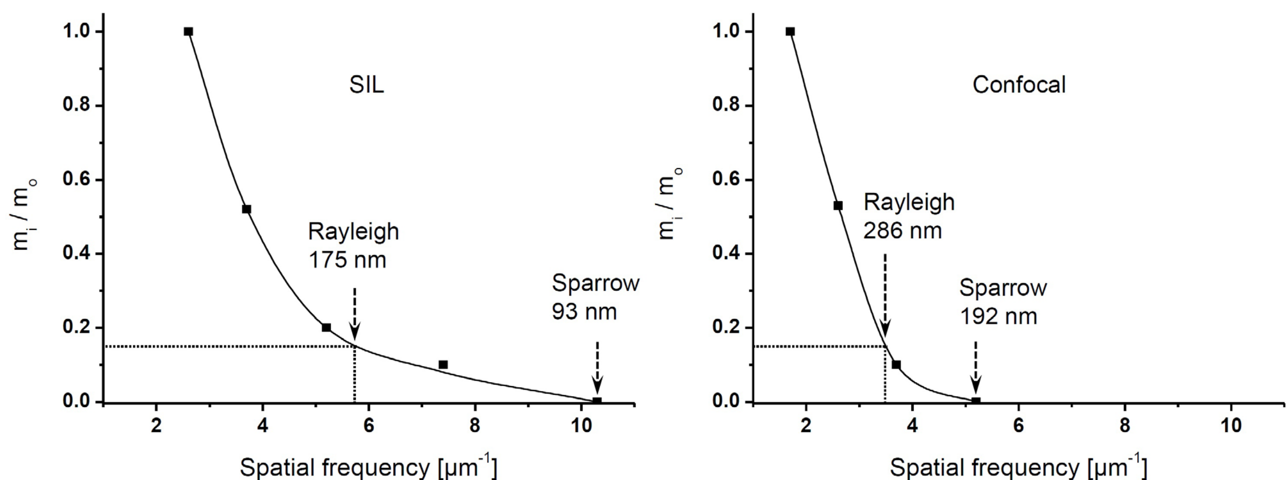

Figure 6: Modulation transfer function m_i / m_o (black squares) for SIL Raman mode (left) and confocal Raman mode (right) determined from the measurements of the BAM L-200 reference pattern. The resolution limits according to the criteria of Rayleigh (m_i / m_o = 0.15) and Sparrow (m_i / m_o ≥ 0) are indicated.

Bereitgestellt von | Hochschule Reutlingen
Angemeldet
Heruntergeladen am | 01.10.15 12:18

The integration of the SIL into a confocal Raman microscope allows convenient Raman imaging and spectroscopy with super-resolution. The lateral resolution in the Raman imaging mode with the actual SILs is determined by means of the modulation transfer function to approximately 180 nm on the basis of the Rayleigh criteria and approximately 90 nm on the basis of the Sparrow criteria, each with 532 nm laser illumination. The lateral resolution is not purely an instrument property, but also depends strongly on the sample characteristics. Here, the BAM L-200 reference pattern turns out to be highly beneficial. In summary, the lateral resolution of the SIL in the Raman mode is significantly beyond the classical diffraction limit of Abbe. For a higher resolution, a more efficient isolation of the evanescent parts of the Raman light is required.

The SIL concept improves the S/N ratio in comparison to aperture-limited systems. A SIL probe with a spot size of approximately 100 nm transmits about 50% of the optical power [25, 28, 38]. By comparison, a metal-coated fiber-probe with a 100 nm aperture transmits only a fraction (10^{-3} - 10^{-6}) of the light coupled into the fiber [16,39-41].

This access to the near-field might be managed by two possible approaches. One is the illumination side. Here, it can be beneficial to switch from a linearly polarized laser beam to a radially polarized one, e.g. with a 4Pi setup. A dark field illumination of the SIL may also be advantageous. The other approach is an optimized manufacturing method for smoother surfaces of the SIL. Our SILs are produced with classical grinding technology resulting in surface scratches and major inhomogeneities. Microelectronic fabrication procedures could help to reduce variations and standardize the lenses. Plastic molding methods for micro and nano-SILs could be very efficient. Precise prototypes in low numbers could be produced with the gold FIB technique. Using GRIN lenses as starting point for SIL development also seems reasonable.

Furthermore, the SIL mode conserves the substrate compared to the high light intensities on the substrate in the confocal imaging mode without SIL.

Acknowledgement: We acknowledge the financial support by Deutsche Forschungsgemeinschaft, DFG, grant no. 581569 and 582923.

References

[1] Mansfield, S. M.; Kino, G. S., Solid immersion microscope. *Applied Physics Letters* 1990, *57* (24), 2615-2616.

[2] Mansfield, S. M.; Studenmund, W. R.; Kino, G. S.; Osato, K., High-numerical-aperture lens system for optical storage. *Optics letters* 1993, *18* (4), 305-307.

[3] Matsuo, S.; Misawa, H., Direct measurement of laser power through a high numerical aperture oil immersion objective lens using a solid immersion lens. *Review of Scientific Instruments* 2002, *73* (5), 2011-2015.

[4] Milster, T. D.; Akhavan, F.; Bailey, M.; Erwin, J. K.; Felix, D. M.; Hirota, K.; Koester, S.; Shimura, K.; Zhang, Y., Super-Resolution by Combination of a Solid Immersion Lens and an Aperture. *Japanese Journal of Applied Physics* 2001, *40* (Part 1, No. 3B), 1778-1782.

[5] Chau, Y.-F.; Yang, T.-J.; Tsai, D. P., Near-field optics simulation of a solid immersion lens combining with a conical probe and a highly efficient solid immersion lens-probe system. *Journal of Applied Physics* 2004, *95* (7), 3378-3384.

[6] Ippolito, S. B.; Goldberg, B. B.; Unlu, M. S., Theoretical analysis of numerical aperture increasing lens microscopy. *Journal of Applied Physics* 2005, *97* (5), 053105-12.

[7] Bischoff, J.; Brunner, R., Numerical investigation of the resolution in solid immersion lens systems. *Proceedings of SPIE* 2000, *4099* (1), 235.

[8] Milster, T. D.; Jo, J. S.; Hirota, K., Roles of Propagating and Evanescent Waves in Solid Immersion Lens Systems. *Applied Optics* 1999, *38* (23), 5046-5057.

[9] Ippolito, S. B.; Terada, H., *Annular illumination and collection in solid immersion*, In International Symposium for Testing and Failure Analysis ISTFA, San Jose, CA, ASM International Materials Park, Ohio: San Jose, CA, 2009; pp 60-64.

[10] Ostertag, E.; Merz, T.; Kessler, R. W., Multimodal spatially resolved near-field scattering and absorption spectroscopy. *Proceedings of SPIE* 2012, *8231*, 82310A-1-82310A-10.

[11] Koyama, K.; Yoshita, M.; Baba, M.; Suemoto, T.; Akiyama, H., High collection efficiency in fluorescence microscopy with a solid immersion lens. *Applied Physics Letters* 1999, *75* (12), 1667-1669.

[12] Kim, M.-S.; Scharf, T.; Brun, M.; Olivier, S.; Nicoletti, S.; Herzig, H. P., Advanced optical characterization of micro solid immersion lens. *Proceedings of SPIE* 2012, *8430*, 84300E-1-84300E-10.

[13] Kim, M.-S.; Scharf, T.; Haq, M. T.; Nakagawa, W.; Herzig, H. P., Subwavelength-size solid immersion lens. *Optics letters* 2011, *36* (19), 3930.

[14] R. Brunner; Dobschal, H. J., Diffractive Optical Lenses in Imaging Systems–High-Resolution Microscopy and Diffractive Solid Immersion Systems. In *Optical Imaging and Microscopy: Techniques and Advanced Systems*, 2nd edition ed.; Török, P.; Kao, F.-J., Eds. Springer: Heidelberg, 2007; pp 45-70.

[15] Frey, H. G.; Bolwien, C.; Brandenburg, A.; Ros, R.; Anselmetti, D., Optimized apertureless optical near-field probes with 15 nm optical resolution. *Nanotechnology* 2006, *17*, 3105-3110.

[16] Goldberg, B. B.; Ippolito, S. B.; Novotny, L.; Liu, Z.; Ünlü, M. S., Immersion Lens Microscopy of Photonic Nanostructures and Quantum Dots. *IEEE Journal of Selected Topics in Quantum Electronics* 2002, *8* (5), 1051-1059.

[17] Terris, B.; Mamin, H. J.; Rugar, D.; Studenmund, W.; Kino, G. S., Near-field optical data storage using a solid immersion lens. *Applied Physics Letters* 1994, *65* (4), 388-390.

[18] Daiichi, K.; Takeshi, K.; Ryuji, S.; Haruki, T.; Yoshimichi, T.; Kiyoshi, O., Near-Field Optical Recording Using Solid

Bereitgestellt von | Hochschule Reutlingen
Angemeldet
Heruntergeladen am | 01.10.15 12:18

Immersion Lens for High-Density Flexible Optical Disks. *Japanese Journal of Applied Physics* 2013, *52* (9S2), 09LG01.
[19] Park, K.-S.; Kim, T.; Lee, W.-S.; Joe, H.-E.; Min, B.-K.; Park, Y.-P.; Yang, H.; Kang, S.-M.; Park, N.-C., Application of Solid Immersion Lens-Based Near-Field Recording Technology to High-Speed Plasmonic Nanolithography. *Japanese Journal of Applied Physics* 2012, *51*, 08JF01-08JF07.
[20] Park, N.-C.; Young-Pil, P.; Park, K.-S.; Hyunseok, Y., Applications of Next Generation Optical Data Storage Technologies. *IEEE Transactions on Magnetics* 2011, *47* (3), 669-678.
[21] Ishimoto, T.; Aki, Y.; Kondo, T.; Kishima, K.; Yamamoto, K.; Yamamoto, M., Near-Field Optical Head for Disc Mastering Process. *Japanese Journal of Applied Physics* 2000, *39* (Part 1, No. 2B), 800-805.
[22] Ippolito, S. B.; Goldberg, B. B.; Unlu, M. S., High spatial resolution subsurface microscopy. *Applied Physics Letters* 2001, *78* (26), 4071-4073.
[23] Dozor, D. M.; Kim, Y.; Tumidajski; Fancher, G.; Salvestrini, K.; Holt, d.; DeWitt, R. Inspection system ultilizing solid immersion lenses. Patent US020120092655A1, 2012.
[24] Merz, T.; Kessler, R. W., Spectroscopic Imaging in the Near Field with an Apertureless Solid Immersion Lens Microscope. *Proceedings of SPIE* 2007, *6631*, 66310V-1 - 6631V-10.
[25] Wu, Q.; Ghislain, L. P.; Elings, V. B., Imaging with solid immersion lenses, spatial resolution, and applications. *Proceedings of the IEEE* 2000, *88* (9), 1491 - 1498.
[26] Karrai, K.; Lorenz, X.; Novotny, L., Enhanced reflectivity contrast in confocal solid immersion lens microscopy. *Applied Physics Letters* 2000, *77* (21), 3459-3461.
[27] Wildanger, D.; Patton, B. R.; Schill, H.; Marseglia, L.; Hadden, J. P.; Knauer, S.; Schönle, A.; Rarity, J. G.; O'Brien, J. L.; Hell, S. W.; Smith, J. M., Solid Immersion Facilitates Fluorescence Microscopy with Nanometer Resolution and Sub-Ångström Emitter Localization. *Advanced Materials* 2012, *24* (44), OP309-OP313.
[28] Ghislain, L. P.; Elings, V. B.; Crozier, K. B.; Manalis, S. R.; Minne, S. C.; Wilder, K.; Kino, G. S.; Quate, C. F., Near-field photolithography with a solid immersion lens. *Applied Physics Letters* 1999, *74* (4), 501-503.
[29] Kino, G., Applications and theory of the solid immersion lens. *Proceedings of SPIE* 1999, *3609* (1), 56-65.
[30] Vollmer, M.; Giessen, H.; Stolz, W.; Rühle, W. W.; Ghislain, L.; Elings, V., Ultrafast nonlinear subwavelength solid immersion spectroscopy at T=8K. *Applied Physics Letters* 1999, *74* (13), 1791-1793.
[31] Hartschuh, A.; Sánchez, E. J.; Xie, X. S.; Novotny, L., High-Resolution Near-Field Raman Microscopy of Single-Walled Carbon Nanotubes. *Physical Review Letters* 2003, *90* (9), 095503.
[32] Lerman, G. M.; Israel, A.; Lewis, A., Applying solid immersion near-field optics to Raman analysis of strained silicon thin films. *Applied Physics Letters* 2006, *89* (22), 223122.
[33] Athalin, H.; Lefrant, S., Optically addressable selective nanovolume Raman spectroscopy of nanoparticles. *Journal of Nanoparticle Research* 2005, *7* (1), 89-93.
[34] Desmedt, A.; Talaga, D.; Bruneel, J. L., Enhancement of the Raman Scattering Signal Due to a Nanolens Effect. *Applied Spectroscopy* 2007, *61* (6), 621-623.
[35] Poweleit, C. D.; Gunther, A.; Goodnick, S.; Menéndez, J., Raman imaging of patterned silicon using a solid immersion lens. *Applied Physics Letters* 1998, *73* (16), 2275-2277.
[36] Brunner, R.; Burkhardt, M.; Pesch, A.; Sandfuchs, O.; Ferstl, M.; Hohng, S.; White, J. O., Diffraction-based solid immersion lens. *Journal of the Optical Society of America A* 2004, *21* (7), 1186-1191.
[37] Ghislain, L. P.; Elings, V. B., Near-field scanning solid immersion microscope. *Applied Physics Letters* 1998, *72* (22), 2779-2781.
[38] Yoshita, M.; Koyama, K.; Baba, M.; Akiyama, H., Fourier imaging study of efficient near-field optical coupling in solid immersion fluorescence microscopy. *Journal of Applied Physics* 2002, *92* (2), 862-865.
[39] Zayats, A.; Richards, D., *Nano-Optics and Near-Field Optical Microscopy*. Artech House, Inc.: Boston, 2009.
[40] Hecht, B.; Sick, B.; Wild, U. P.; Deckert, V.; Zenobi, R.; Martin, O. J. F.; Pohl, D. W., Scanning near-field optical microscopy with aperture probes: Fundamentals and applications. *The Journal of Chemical Physics* 2000, *112* (18), 7761-7774.
[41] Knoll, B.; Keilmann, F., Electromagnetic fields in the cutoff regime of tapered metallics waveguides. *Optics Communications* 1999, *162*, 177-181.
[42] Ostertag, E.; Merz, T. R.; Kessler, R. W., Imaging beyond diffraction limit - prospectives for the NIR. *Proc. of the 15th International Conference on Near Infared Spectroscopy NIRS 2012* 2013, 41-46.
[43] *Naturwissenschaftliches und Medizinisches Institut (NMI) an der Universität Tübingen*, http://www.nmi.de.
[44] Ghislain, L. P.; Elings, V. B. Scanning probe optical microscope using a solid immersion lens. Patent WO98/58288, 1998.
[45] *Bundesanstalt für Materialforschung*, http://www.rm-certificates.bam.de/de/rm-certificates_media/rm_cert_layer_and_surface/bam_l200e.pdf.
[46] Blakemore, J. S., Semiconducting and other major properties of gallium arsenide. *Journal of Applied Physics* 1982, *53* (10), R123-R181.
[47] Burns, G.; Dacol, F. H.; Wie, C. R.; Burstein, E.; Cardona, M., Phonon shifts in ion bombarded GaAs: Raman measurements. *Solid State Communications* 1987, *62* (7), 449-454.
[48] Chang, Y.-C.; Ren, S.-F.; Wen, G., Raman spectra of GaAs-$Al_xGa_{1-x}As$ superlattices. *Superlattices and Microstructures* 1993, *13* (2), 165-168.
[49] Johnston, W. D. J.; Kaminow, I. P., Contributions to Optical Nonlinearity in GaAs as Determined from Raman Scattering Efficiencies. *Physical Review* 1969, *188* (3), 1209-1211.
[50] Mooradian, A.; Wright, G. B., First order Raman effect in III-V compounds. *Solid State Communications* 1966, *4*, 431-434.
[51] Kubota, K.; Nakayama, M.; Katoh, H.; Sano, N., Characterization of GaAs-AlAs superlattices by laser Raman spectroscopy. *Solid State Communications* 1984, *49* (2), 157-159.
[52] Sood, A. K.; Menéndez, J.; Cardona, M.; Ploog, K., Interface vibrational modes in GaAs-AlAs superlattices. *Physical Review Letters* 1985, *54* (19), 2115-2118.
[53] Fauchet, P. M.; Campbell, I. H., Raman spectroscopy of low-dimensional semiconductors. *Critical Reviews in Solid State and Materials Sciences* 1988, *14* (Sup1), S79-S101.

Bereitgestellt von | Hochschule Reutlingen
Angemeldet
Heruntergeladen am | 01.10.15 12:18

[54] Deutsches Institut für Normung, DIN ISO 9334:2008-08 Optics and photonics - Optical transfer function - Definitions and mathematical relationships. 2008.
[55] Senoner, M.; Wirth, T.; Unger, W. E. S., Imaging surface analysis: Lateral resolution and its relation to contrast and noise. *Journal of Analytical Atomic Spectrometry* 2010, *25* (9), 1440-1452.
[56] Cox, G.; Sheppard, C. J. R., Practical limits of resolution in confocal and non-linear microscopy. *Microscopy Research and Technique* 2004, *63* (1), 18-22.
[57] Sheppard, C. J. R.; Choudhury, A., Image Formation in the Scanning Microscope. *Optica Acta: International Journal of Optics* 1977, *24* (10), 1051-1073.
[58] Cox, I. J.; Sheppard, C. J. R.; Wilson, T., Super-resolution by confocal fluorescent microscopy. *Optik* 1982, *60* (4), 391-396.

Bereitgestellt von | Hochschule Reutlingen
Angemeldet
Heruntergeladen am | 01.10.15 12:18